Temperature study of photoinduced wide-angle scattering in cerium-doped strontium barium niobate

Mikhail Goulkov

Institute of Physics, Science Avenue 46, 03650, Kiev-39, Ukraine

Mirco Imlau and Rainer Pankrath

Fachbereich Physik, Universität Osnabrück, Barbarastrasse 7, D-49069 Osnabrück, Germany

Torsten Granzow, Udo Dörfler, and Theo Woike

Institut für Mineralogie und Geochemie, Universität zu Köln, Zülpicher Strasse 49b, D-50674 Köln, Germany

Received June 10, 2002; revised manuscript received August 23, 2002

The photoinduced polarization-isotropic scattering in strontium barium niobate (SBN) doped with 0.66-mol. % cerium has been studied over a wide temperature range including the region of the relaxor phase transition. The temperature evolution of the scattering pattern has been examined with respect to changes in the domain structure and of optical parameters of the crystal resulting from the phase transition from a ferroelectric state to a paraelectric state. The scattering properties at temperatures above the ferroeletric phase are connected to the relaxor behavior of SBN. We found that a transition temperature T_C can be defined from the temperature evolution of the scattering pattern much more precisely than with conventional methods such as frequency-dependent measurements of the dielectric susceptibility. © 2003 Optical Society of America

OCIS codes: 160.2100, 190.5330, 160.0160.

1. INTRODUCTION

Photoinduced light scattering in photorefractive crystals (PRCs) is a nonlinear optical phenomenon that always accompanies the propagation of a laser beam through a PRC and manifests itself in a variety of light-scattering patterns that differ in spatial structure and orientation of the light polarization.[1–3] The typical photoinduced scattering observed in $Sr_xBa_{1-x}Nb_2O_6$, strontium barium niobate (SBN), is a wide-angle polarization-isotropic scattering from a single extraordinarily polarized laser beam, often referred to as beam fanning.[2] The scattering originates from optical coherent noise exponentially enhanced because of beam coupling between transmitted and scattered waves on parasitic phase gratings formed in the bulk of the crystal.[1] These parasitic gratings are spatial modulations of the refractive index recorded by the pump beam with primary scattering by means of the photorefractive effect.[4] The study of photoinduced scattering has both applied and fundamental aspects: first, knowledge of the processes from which light scattering originates can give a solution for how to eliminate or at least to reduce the scattering and to make PRCs more suitable for industrial applications. Second, photoinduced scattering is a clear fingerprint of the fundamental photorefractive processes in ferroelectric crystals. The study of photoinduced scattering can provide information about a wide range of material parameters including ferroelectric properties of a particular crystal that exhibits this phenomenon.[5,6] Recently, considerable lowering of the phase transition temperature was reported for SBN crystals doped with various concentrations of cerium. Here the transition temperature is reduced from 87 °C for undoped samples of the congruently melting composition ($x = 0.61$, SBN61) to approximately 22 °C in samples doped with 2.07-mol. % cerium.[7] This fact makes it attractive to examine the phase transition in highly doped SBN:Ce by a temperature study of beam fanning. An approach of the actual temperature of the sample to the transition temperature results in anomalous changes of the dielectric constant and the electro-optic coefficients. This should enhance the photoinduced scattering considerably, making it sensitive to changes in the structure of SBN:Ce in the vicinity of the phase transition. The other interesting point is the determination of the phase transition temperature in SBN:Ce as the actual critical point at which this PRC exhibits strong relaxor properties.

SBN belongs to the tungsten bronze family of ferroelectrics[8] and exhibits a typical relaxor kind of behavior at the phase transition from the paraeletric phase to the ferroelectric phase. This means that the polarization in SBN exists locally even far above the phase transition. These so-called polar clusters turn into ferroelectric domains below the phase transition temperature.[9,10] The relaxor behavior and the peculiarities of the domain structure in SBN at high temperatures are satisfactorily explained by the random-field Ising model.[11,12] This model postulates the existence of short-range random electric fields causing a correlation between the dipole

0740-3224/2003/020307-07$15.00

moments of the nanodomains and resulting in the formation of local polar clusters. As a result, a nonzero spontaneous polarization can be observed above the critical temperature. The critical behavior in the ferroelectric relaxor SBN was first experimentally proved by Dec *et al.*[13] and by Kleemann *et al.*[14] A persistence of the local polarization far above the ferroelectric state results in a significantly smeared phase transition, which makes it difficult to detect the actual value of the Curie temperature T_C at which critical changes in the domain structure take place. In ferroelectric relaxors, the term phase transition temperature is often applied to the temperature T_m, which corresponds to the maximum of the experimentally measured temperature dependence of the dielectric permittivity. Since this method allows measurement of only the integrated response of the crystal to temperature changes, the T_m value strongly depends on the history with regard to the electric field poling of the sample. For the first time to our knowledge, the temperature T_C in SBN was detected from measurements of the linear birefringence dependent on temperature.[10]

Here we present new results of photoinduced light scattering in highly doped SBN61:Ce experimentally studied over a wide temperature range that covers the ferroelectric, relaxor, and paraelectric phases. The temperature evolution of beam fanning is examined in detail and is interpreted within the framework of the photorefractive model that describes beam fanning, in which the relaxor properties of SBN are taken into account. Experimentally, beam fanning is observed with respect to its spatial distribution and integral intensity from the ferroelectric phase at room temperature up to 140 °C far into the paraelectric phase. The integral scattered intensity increases strongly in the $T < T_C$ temperature range when it heats up. If the crystal passes into the relaxor state at $T > T_C$, the gradual missequencing of the domain structure initiates changes in the spatial distribution and reduces the integral intensity of the scattered light. At temperatures $T \gg T_C$, when the crystal is in the paraelectric phase, photoinduced light scattering vanishes completely. One can detect the value of T_C from the temperature dependence of the spatial distribution of the scattering pattern by defining an asymmetry parameter.

2. EXPERIMENTAL SETUP

A single crystal of SBN61 doped with 0.66-mol. % cerium was grown by use of the Czochralski technique. We prepared a rectangular parallelepiped with the edges cut parallel to the crystallographic axes and with dimensions of 0.895 mm × 7.15 mm × 6.2 mm along the a, b, and c axis, respectively. We poled the sample electrically by heating it up to 140 °C, applying an external electric field of 350 V/mm along the c axis, and then slowly cooling it to room temperature before we removed the field. To change and to control the temperature of the crystal during the measurements in the range from +10 to +150 °C, we mounted the holder on a thermoelectric element. A temperature controller allowed us to adjust the sample temperature to an absolute accuracy of 0.3 °C. The surfaces of the crystal normal to the c axis were short circuited to prevent the influence of the pyroelectric effect. A sketch of the setup is shown in Fig. 1(a). The beam of a He–Ne laser ($\lambda = 633$ nm) serves as a pump beam and is directed onto the crystal normal to the large a face of the sample. An extraordinary light polarization was chosen. The beam intensity was adjusted to a value of 70 mW/cm^2 by use of a half-wave retarder plate and a Glan–Thompson prism. The absorption coefficient is measured to 4 cm^{-1} at $\lambda = 633$ nm. A small fraction of the pump beam is directed onto photodiode PD1 by a beam splitter to monitor the intensity of the pump beam. Photodiode PD2 is mounted on a motorized rotating stage at a distance of $d = 5.5$ cm behind the sample. Thus, it is possible to scan the scattering pattern in an exact half-circle around the sample in the direction from the negative to the positive end of the polar axis of the crystal. The scattered light distribution behind the crystal is measured in the range of scattering angles θ_s from −90° to +90° outside the crystal. The aperture of the diaphragm mounted on PD2 limits the apex angle of the measured scattering to 0.5°. Negative and positive angles correspond to scattering inverse to and along the direction of the c axis of the crystal. At $\theta_s = 0°$, the photodiode crosses the pump beam behind the crystal. The entire setup is enclosed in a black box (represented by the dotted rectangle in Fig. 1). The pump beam passes through a small opening of the black box, so as to mini-

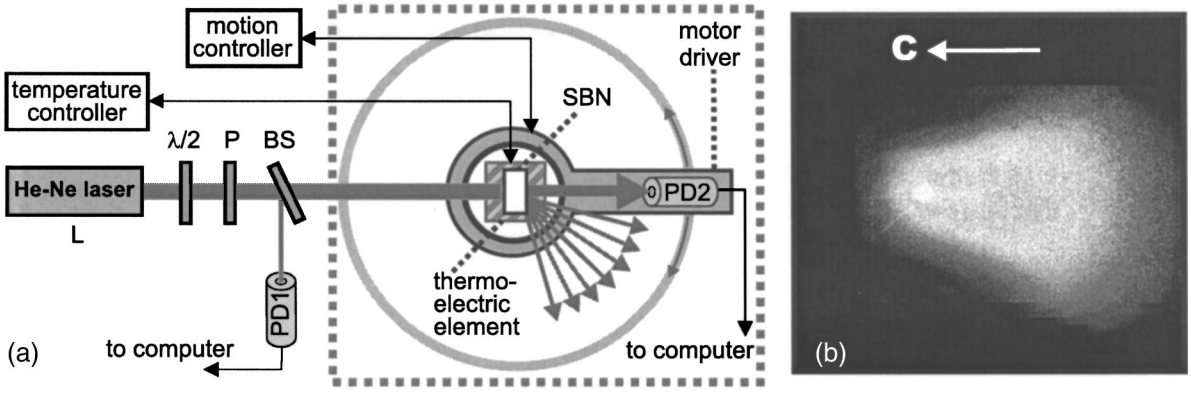

Fig. 1. (a) Experimental setup for measuring the angular distribution of scattered light at different temperatures: L, He–Ne laser; λ/2, half-wave retarder plate; P, Glan–Thompson prism; BS, beam splitter; PD1, PD2, photodetectors. The SBN61:Ce (0.66-mol. %) sample was placed on a stack of thermoelectric elements to regulate the temperature. (b) Typical scattering pattern of SBN61:Ce (0.66 mol. %). The bright spot marks the transmitted laser beam.

mize the background noise that is due to external light sources.

3. EXPERIMENTAL RESULTS

During the illumination of SBN:Ce with an extraordinarily polarized coherent beam, a photoinduced light scattering appears behind the crystal distributed in the vicinity of the directly transmitted beam and having the same light polarization as the incident beam. The light pattern formed by the scattered light on a screen is shown in Fig. 1(b). The arrow shows the direction of the polar c axis. The typical time necessary to reach a steady-state distribution of the scattering pattern at room temperature at a given intensity of the pump beam is approximately 10–15 min. Figure 2 shows the one-dimensional angular profile of the stationary intensity distribution of this pattern (crystal temperature of $T = 28\,^{\circ}\mathrm{C}$) as a solid curve labeled a. The sharp intensity peak in the central part of the scan corresponds to the directly transmitted pump beam. Because of the small aperture of the diaphragm on photodiode PD2, this peak is only a section of the beam cut by the diaphragm. The dashed curve labeled b represents the angular profile of the pump beam without a sample. Both intensity profiles are normalized to their maximum intensities $I_{\max}$. The angular distribution of the light pattern as well as the pattern in Fig. 1(b) is strongly asymmetric. The main part of the scattered light is found at negative scattering angles θ_s, which corresponds to the direction opposite the c axis ($-c$ direction). Scattering in the $-c$ direction exhibits a wide and not well-pronounced maximum at angle $\theta_s^{I\max} = -(30 \pm 5)^{\circ}$. The scattering measured along the c axis (positive scattering angles or $+c$ direction) is rather weak. To obtain a quantitative measure of the asymmetry of the scattering distribution, we introduce the asymmetry coefficient $m_{\mathrm{as}} = I_-/I_+$ defined as the intensity ratio of the scattering in the $-c$ direction and in the $+c$ direction. I_- and I_+ are the integral scattering intensities in the $-c$ and $+c$ directions measured in the steady state and shown in Fig. 2 by the two crosshatched areas below the intensity curve. The angular interval $-2^{\circ} \leqslant \theta_s \leqslant 2^{\circ}$ is excluded from the calculation of I_+ and I_- to take into account the scattered light only. The measured asymmetry coefficient for the scattering profile shown in Fig. 2 is $m_{\mathrm{as}} = 14.3$. This study of photoinduced scattering was carried out for different temperatures in the range from $+15$ to $+148\,^{\circ}\mathrm{C}$. When the crystal is cooled to temperatures lower than room temperature, the maximum of the scattering pattern becomes flatter and the integral scattering intensity decreases.

The temperature evolution of the scattering pattern with increasing temperature can be divided into three phases or steps with respect to the fact that SBN undergoes the transition from the ferroelectric into the paraelectric phase passing through the relaxor (or precursor) phase. These three phases are illustrated in Fig. 3 by three angular scans at $T = 50\,^{\circ}\mathrm{C}$ (solid curve), $T = 58\,^{\circ}\mathrm{C}$ (long dashed curve), and $T = 90\,^{\circ}\mathrm{C}$ (short dashed curve), respectively. The results of the temperature study of photoinduced scattering in SBN are further

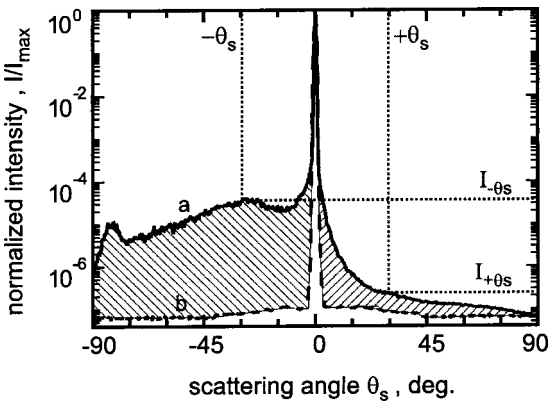

Fig. 2. a, Typical angular distribution of the scattered light in SBN at $T = 28\,^{\circ}\mathrm{C}$ in the plane spanned by the c axis and the laser beam. The central peak is the transmitted laser beam. The two crosshatched areas to the left and to the right of the peak are taken to derive the integral intensities in the $-c$ and $+c$ directions of the scattering profile, respectively. The intensities $I_{+\theta s}$ and $I_{-\theta s}$ correspond to two symmetric scattering angles, where $\pm\theta_s$ is defined by the maximum of the intensity of the scattering pattern. b, Beam profile without a sample, representing the noise of the system.

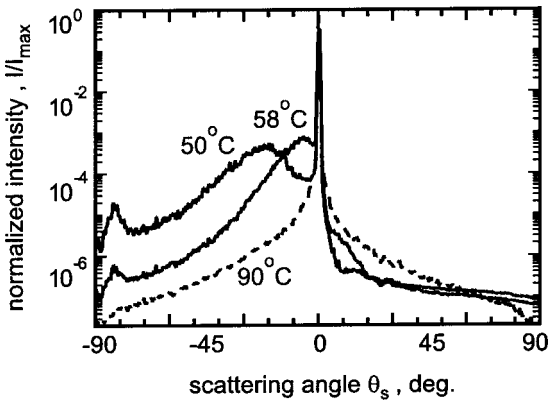

Fig. 3. Angular distribution of the scattered light in SBN in the ferroelectric state ($T = 50\,^{\circ}\mathrm{C}$), the relaxor state ($T = 58\,^{\circ}\mathrm{C}$), and the paraelectric state ($T = 90\,^{\circ}\mathrm{C}$).

presented in detail in Figs. 4–6. Figure 4(a) shows the transmitted pump intensity I_p, and Fig. 4(b) shows the integrated intensity $I_\Sigma = I_- + I_+$ of the scattered light obtained from the angular scan. To show only the temperature dependence of the curves, they have been normalized to their maximum values. Figure 5 shows the temperature dependence of the asymmetry coefficient m_{as} over the whole temperature range. Figure 6 shows the angular position of the maximum of the scattered intensity dependent on temperature, for which the angles were derived from the corresponding angular profiles of the scattered light. The experimental results are displayed by filled rectangles. In the first phase from low temperatures to approximately 52 °C, the total scattered intensity increased nonlinearly. Additionally, the transmitted pump beam decreased. The scattering intensity grows in the $-c$ direction and drops in the $+c$ direction, leading to a sharp increase of the asymmetry coefficient. The peak of the scattering intensity in the angular scan becomes sharper and moves closer to the pump beam. The basic features of the first phase are illustrated in Figs. 4 and 5.

They are characterized by a drastic drop of I_p, by a fast nonlinear growth of the I_Σ curves and also of m_{as} in the temperature range up to $T = 52\,^\circ\mathrm{C}$.

The second phase begins at $T \geqslant 52\,^\circ\mathrm{C}$ and continues to approximately $T = 65\,^\circ\mathrm{C}$. In this phase, the total scattering intensity starts to decrease, whereas the intensity of the transmitted pump beam increases. The decrease of the scattered intensity is especially pronounced for large angles in both directions, whereas the scattered intensity for small angles still shows a large maximum. In this phase, the fast decay of the asymmetry of the scattering pattern takes place, intensity I_- decreases and I_+ increases, resulting in a pronounced maximum of the asymmetry coefficient. The position of the maximum of the scattering profile continues to move to smaller scattering angles and finally merges with the pump beam at approximately $T = 65\,^\circ\mathrm{C}$, where it can no longer be observed. The scattering intensity and the asymmetry coefficient are reduced to values that are comparable with those at room temperature.

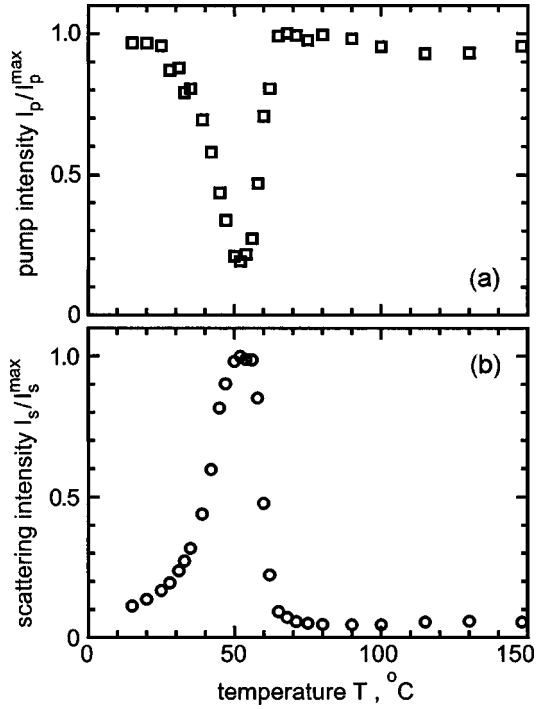

Fig. 4. (a) Temperature dependence of the transmitted pump intensity. (b) Temperature dependence of the total scattered intensity $I_\Sigma = I_- + I_+$. Both curves have been normalized to their maximum values.

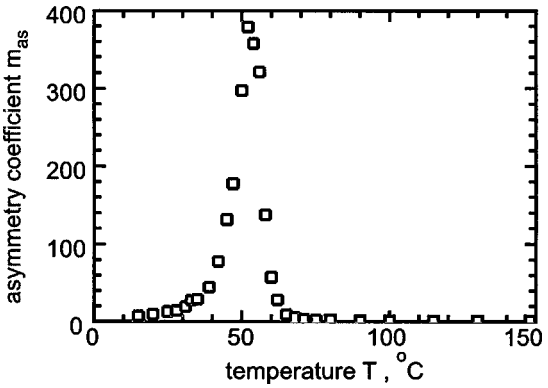

Fig. 5. Dependence of the asymmetry coefficient $m_{as} = I_-/I_+$ on the temperature.

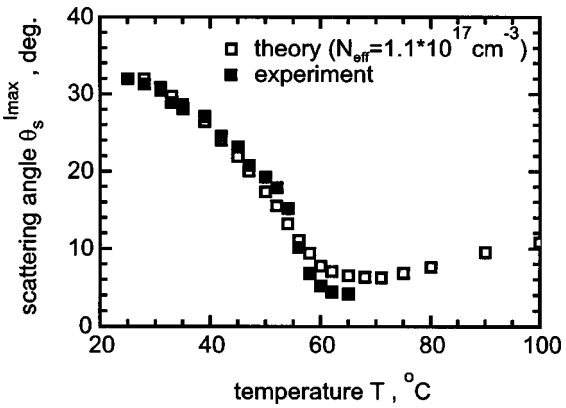

Fig. 6. Temperature dependence of the angular position of the maximum of the scattered intensity. Filled and open squares represent the experimental and theoretical values ($N_{eff} = 1.1 \times 10^7\ \mathrm{cm}^{-3}$), respectively.

At $T = 65\,^\circ\mathrm{C}$, the third and last phase of the temperature development of the scattering starts. The transmitted pump intensity continues to increase and the total scattered intensity continues to decrease, but at a much slower rate than in the previous phase. At $T = 100\,^\circ\mathrm{C}$ the photoinduced scattering practically vanishes into the background noise. The asymmetry coefficient in the third phase becomes much smaller compared with the room-temperature values and finally falls to unity for $T \geqslant 100\,^\circ\mathrm{C}$, indicating an absolutely symmetric angular distribution of the scattered light. This phase of the temperature evolution of the scattering is illustrated by slow tails of the curves in Figs. 4 and 5.

Finally it should be noted that the scattering exhibits a reversibility with respect to the heating and cooling procedures. When the crystal is cooled to room temperature, the scattering maximum reappears and the light pattern becomes asymmetric again. The evolution of the scattering in this case passes the above-mentioned three phases in reverse order.

4. DISCUSSION

Photoinduced light scattering from an extraordinarily polarized pump beam (beam fanning) is observed in SBN in the ferroelectric phase up to the regime of the phase transition and disappears in the paraelectric phase. The cause of the scattering process is usually assumed to be optical coherent noise, which is nonlinearly amplified by means of two-beam coupling processes at the expense of the pump beam.[1] The primary seed scattering is a part of the incident light scattered from imperfections of the surface and the bulk (including the domain structure) of the crystal and is characterized by a wide angular indicatrix. The scattered light interferes with the transmitted part of the incident beam and forms a rather complicated light field. It stems from a linear superposition of a huge number of elementary light patterns arbitrarily oriented in space. One elementary pattern is formed by a pair of

transmitted (pump) and scattered (seed) light waves that consists of bright and dark fringes periodically sequenced along the grating vector $K_g = 2\pi/\Lambda = 4\pi \sin \theta_s^{\text{in}}/\lambda$, where θ_s^{in} denotes the angle between the seed and the pump components inside the crystal. Exposure of SBN to such elementary light gratings results in a nonuniform photoexcitation of electrons into the conduction band, in their migration caused by thermal diffusion from bright regions, their trapping in dark regions, and finally in the formation of a spatially modulated electric field. The spatial structure of the space–charge field formed by diffusion processes is shifted in space by $\Lambda/4$ with respect to the initiating interference light pattern. The amplitude of the electric space–charge field can be expressed[15] as

$$E_{\text{sc}} = \frac{m k_B T}{e} \times \frac{K_g}{(1 + (K_g/K_d)^2)} \times \hat{e}_p \hat{e}_s , \qquad (1)$$

where k_B is Boltzmann's constant, T is the temperature, e is the unit charge, m is the modulation depth of the light interference pattern, and $\hat{e}_p$, $\hat{e}_s$ are unit vectors of the polarization of electric fields of the pump and scattered waves, respectively. The expression for the inverse Debye-screening length K_d is given by

$$K_d = \frac{e^2 N_{\text{eff}}}{(\epsilon_{33}\epsilon_0 k_B T)^{1/2}}, \qquad (2)$$

where N_{eff} is the trap density, ϵ_{33} and ϵ_0 are, respectively, the dielectric permittivity and the dielectric constant.

The linear electro-optic effect (Pockels effect) present in the polar phase of SBN transfers this modulation of the space–charge field into a spatial modulation of the refractive index. The amplitude of the resulting refractive-index grating is proportional to the amplitude of the space–charge field[4]:

$$\Delta n = -\frac{1}{2} n_{\text{eff}}^3 r_{\text{eff}} E_{\text{sc}} . \qquad (3)$$

For beam-fanning gratings formed in SBN, the effective refractive index is, in good approximation, $n_{\text{eff}} \approx n_e$, and the effective electro-optic coefficient is

$$r_{\text{eff}} \approx r_{33} = 2\epsilon_0 \epsilon_{33} g_{33} P_3 , \qquad (4)$$

where $P_3 = P_S$ is the spontaneous polarization and g_{33} is the quadratic electro-optic coefficient. An interaction of the pair of pump and scattered waves on the shifted grating results in a stationary energy transfer that takes place in the direction opposite the grating shift. In SBN, the light scattered in the $-c$ direction is amplified and the light scattered in the $+c$ direction is depleted, forming a unidirectional scattering pattern oriented inverse to the c axis [see Fig. 1(b) and Fig. 3]. The amplification–depletion processes exponentially depend on crystal thickness l, and in the steady state the scattered wave with initial intensity I_{so} reaches the value $I_s = I_{so} \exp(\Gamma l)$. Gain factor Γ describes the nonlinear properties of the medium and can be written[16] as

$$\Gamma_{\pm c} = \pm \frac{4\pi \Delta n}{\lambda m \cos \theta_s} = \mp \frac{2\pi n_e^3 r_{33}}{\lambda m} \left(\frac{E_{sc}}{\cos \theta_s} \right), \qquad (5)$$

where the + sign applies to waves scattered in the $-c$ direction and the − sign to waves scattered in the $+c$ direction. The sign of the electro-optic coefficient r_{33} in Eq. (5) is considered to be positive for the whole crystal, assuming that the vector of the spontaneous polarization P_S is constant across the bulk of the crystal. This is true only for ideal nonconducting ferroelectrics kept at $T < T_C$. Microdefects (including doping ions) and nonzero conductivity result in a rather complicated domain structure in a sample. Real ferroelectrics usually consist of a vast number of needlelike ferroelectric domains of different sizes. The spatial orientation of ferroelectric domains in SBN can vary only in two opposite directions antiparallel to each other, resulting in local regions with opposite orientation of the polarization vector. Regions with inverted P_S result either in a reduction of the electro-optic coefficient r or even in the local inversion of its sign. The changes of the electro-optic properties of the crystal necessarily result in similar changes of gain factor Γ, causing a decrease of the total scattered intensity and/or a redistribution of the scattered light in the $\pm c$ directions. The procedure of poling the crystal by an external electric field greatly improves the spatial ordering of the domain structure, causing a significant enhancement of the scattering and its asymmetry. Nonetheless, even a sample prepared as described in Section 2 displays a certain amount of scattering in the direction of the c axis. This indicates that some areas of the domains oriented in the direction opposite the macroscopic polarization exist in the poled crystals and contribute to the angular distribution of the scattered light. When a poled ferroelectric crystal approaches the phase transition temperature, the domain structure becomes unstable, and all optical parameters endure anomalously large changes. Drastic changes of the dielectric constant and the electro-optic coefficient, which is proportional to both the dielectric constant and the spontaneous polarization P_S [approximation (4)], result in a strong alteration of the gain factor in the vicinity of T_C. The strong increase of the total scattered intensity observed in Fig. 4(b) reflects a competition of the temperature changes of ϵ_{33} and P_3 in Γ.

Owing to the relaxor-type nature of the phase transition, the photoinduced scattering in SBN can be observed even in this intermediate phase. The relaxor behavior of SBN is explained by Westphal *et al.* and by Kleemann *et al.*[11,12] with randomly distributed electric fields that stabilize the domain structure. The randomly distributed electric fields are caused by charge fluctuations that possibly originate from the structural disorder in SBN and favor the existence of polar clusters in a certain temperature interval above the phase transition temperature. In the immediate proximity of T_C, the stabilizing action of randomly distributed electric fields is sufficiently strong, but a further increase of the sample temperature causes the missequencing and then the disruption of the domain structure. The study of the temperature evolution of beam fanning allows us to assume that spatial disordering takes place first for small polar clusters and then for large polar clusters. As a consequence, the large-angle fanning that originates from primary scattering from small-scale structures disappears first. At small angles, the light scattered from large-scale structures ac-

cumulates to increase temperatures and vanishes only at very high temperatures. We assume that temperature T_C is defined as the temperature at which a well-defined domain structure breaks down into disordered polar clusters that are characteristic of the relaxor state. We consider the relaxor phase as a dynamic intermediate state between the ferroelectric and the paraelectric stationary phases. In this state, SBN can no longer be considered to be truly ferroelectric. However, the existence of local randomly distributed electric fields prevents the total decay of the domain structure. The action of these fields is overcome by kinetic disordering at high temperatures. Within this context, it is quite interesting to compare the temperature dependencies of the total scattered intensity I_Σ [Fig. 4(b)] with the asymmetry coefficient m_{as} (Fig. 5). The initial increase of both curves reflects the increase of Γ that is due to the changes of ϵ_{33} and P_3 when T approaches T_C. As a result, the amplification and depletion processes in the $-c$ and $+c$ directions of the scattered light are nonlinearly with increasing temperature. The coefficient m_{as} that measures the ratio of scattering intensities in the $\pm c$ directions exhibits better sensitivity of the temperature increase of Γ than the total scattered intensity I_Σ that evaluates the integrated response. The descending part of the curves reflects the reduction of the Γ value that is due to the decrease of ϵ_{33} and P_3 when the crystal reaches the relaxor phase. In the relaxor phase, the long-range correlation of the ferroelectric domains is substituted by short-range correlations that form polar clusters, for while the mutual orientation of nanodomains is locally correlated by strong randomly distributed electric fields that prevent polar clusters from disruption, but the clusters can flip and thus inverse their orientation. This disordering of the domain structure begins at T_C and results in a redistribution of the scattered light with respect to the $\pm c$ directions and in the reduction of the asymmetry coefficient m_{as}. However, it almost does not affect the total scattering intensity. When the temperature is increased, the process of cluster breakup begins, which results in the real degradation of the domain structure of SBN and in the decrease of Γ. The latter leads to a reduction of the total scattering intensity and of the scattering asymmetry.

These processes, inversion and flipping and breakup of domains, explain the behavior of curves $I_\Sigma(T)$ and $m_{\mathrm{as}}(T)$ in their maxima. The flattened maximum of $I_\Sigma(T)$ corresponds to the process of inversion and flipping of polar clusters. It is similar to the maximum observed for the temperature dependence of the dielectric constant and the linear electro-optic coefficients. The following decrease of $I_\Sigma(T)$ is due to cluster breakup processes. Since the asymmetry of the scattering pattern depends both on the inversion and on the breakup of the polar clusters, the coefficient m_{as} exhibits a stronger dependence on the temperature, falling down when the process of cluster inversion starts. From this we can assume that the maximum of curve $m_{\mathrm{as}}(T)$ corresponds closely to the actual value of T_C in SBN, whereas the maximum of curve $I_\Sigma(T)$ is an analog to T_m, which is usually measured from the dependence $\epsilon_{33}(T)$.

We now estimate the temperature region above T_C in which the photorefractive model of beam fanning developed for $T < T_C$ can still be applied. We therefore have calculated the temperature dependence of the maximum angle of the scattering intensity peak $\theta_s^{I_{\max}}$ by using Eq. (5) and compared the obtained result with the corresponding experimental curve in Fig. 6. The term within parentheses in Eq. (5) describes the angular dependence of the gain factor, whereby the space–charge field E_{sc} depends on angle θ_s by means of the grating wave vector K_d and the product $\hat{e}_p\hat{e}_s$. The dependence of the azimuthal distribution of scattered light on the temperature originates from E_{sc}, which depends on the temperature due to k_BT and $\epsilon_{33}(T)$. Note that the temperature dependence of the electro-optic coefficient r_{33} strongly influences the absolute value of Γ but does not effect the angular distribution of the scattering. The temperature dependence of the dielectric constant $\epsilon_{33}(T)$ has been determined by Dec *et al.*[9] For calculation of the dependence $\theta_s^{I\max}(T)$, we must enter the value of the trap density N_{eff} into the expression for E_{sc} in the term K_d [see Eqs. (1) and (2)]. We assume that the intensity of the primary scattering is the same for two symmetric scattering angles, $+\theta_s$ and $-\theta_s$, and the values of Γ for these angles differ only in sign ($\Gamma_{-\theta s} = -\Gamma_{+\theta s} = |\Gamma_{\theta s}|$). A simple logarithmic subtraction of the two corresponding scattering intensities $I_{-\theta s} = I_0 \exp(+|\Gamma_{\theta s}|l)$ and $I_{+\theta s} = I_0\exp(-|\Gamma_{\theta s}|l)$ yields twice the value of the coupling strength $2|\Gamma_{\theta s}|l$. Applying this procedure to the scattering profile measured at room temperature (see Fig. 3) with $|\theta_s^{I\max}| = 30°$ measured as the maximum of the scattering profile, the gain factor $\Gamma_{I_{\max}} = 29\ \mathrm{cm}^{-1}$ is achieved. By using the literature values[9,17,18] $n_e = 2.284$, $\epsilon_{33} = 2103$, and $r_{33} = 333$ pm/V, one can see that the calculated gain factor $\Gamma^{I_{\max}}$ should be reached with the value $N_{\mathrm{eff}} = 1.1 \times 10^{17}\ \mathrm{cm}^{-3}$. Assuming that this value of N_{eff} does not depend on the temperature, we calculated the theoretical curve $\theta_s^{I\max}(T)$ and plotted it as open squares in Fig. 6. The correspondence between the experimental and the theoretical dependencies is quite good up to $T = 56\,°\mathrm{C}$, which shows that the temperature limit occurs at the point at which Eqs. (1) to (5), derived for $T < T_C$, cannot be applied for the temperature range above the phase transition point.

5. CONCLUSION

In conclusion, we have studied the photoinduced polarization-isotropic scattering in SBN61:Ce (0.66 mol. %) over a wide temperature range. The temperature evolution of the spatial distribution of the scattering intensity was discussed with respect to changes in the domain structure when the crystal undergoes a phase transition from the ferroelectric to the paraelectric phase passing the intermediate relaxor state. The scattering observed at temperatures above the phase transition was shown to be due to the relaxor properties of SBN. The scattering asymmetry coefficient m_{as}, defined as the intensity ratio of the light scattered in the direction parallel and antiparallel to the polar axis, was introduced to evaluate changes in the domain structure of the crystal. We have shown that the temperature dependence of the asymmetry coefficient $m_{\mathrm{as}}(T)$ can be used to determine

the value of critical temperature T_C. Our estimations also show that the conventional photorefractive model of photoinduced scattering is valid even at a temperature range above T_C.

ACKNOWLEDGMENT

This research was supported by the Deutsche Forschungsgemeinschaft (DFG), project SPP 1056/WO 618/3-3, and INTAS project 01-0173. M. Goulkov gratefully acknowledges support from the DFG for his stay at the Institut für Mineralogie at the Universität zu Köln.

M. Goulkov's e-mail address is goulkov@iop.kiev.ua.

REFERENCES

1. V. V. Voronov, I. R. Dorosh, Yu. S. Kuz'minov, and N. V. Tkachenko, "Photoinduced light scattering in cerium-doped barium strontium niobate crystals," Sov. J. Quantum Electron. **10**, 1346–1349 (1980).
2. J. Feinberg, "Asymmetric self-defocusing of an optical beam from the photorefractive effect," J. Opt. Soc. Am. **72**, 46–51 (1982).
3. B. Sturman, S. Odoulov, and M. Goulkov, "Parametric four-wave processes in photorefractive crystals," Phys. Rep. **275**, 197–254 (1996).
4. N. V. Kukhtarev, V. B. Markov, S. G. Odulov, M. S. Soskin, and V. L. Vinetskii, "Holographic storage in electrooptic crystals. II. Beam coupling—light amplification," Ferroelectrics **22**, 961–964 (1979).
5. D. Rytz, B. A. Wechsler, R. N. Schwarz, C. C. Nelson, C. D. Brandle, A. J. Valentino, and G. W. Berkstresser, "Temperature dependence of photorefractive properties of strontium-barium niobate ($Sr_{0.6}Ba_{0.4}Nb_2O_6$)," J. Appl. Phys. **66**, 1920–1924 (1989).
6. R. A. Rupp, J. Seglins, and U. van Olfen, "Phase transition of SBN:Ce studied by anisotropic holographic scattering," Phys. Status Solidi B **168**, 445–454 (1991).
7. T. Volk, Th. Woike, U. Dörfler, R. Pankrath, L. Ivleva, and M. Wöhlecke, "Ferroelectric phenomena and holographic properties of strontium-barium-niobate crystals doped with rare-earth elements," Ferroelectrics **203**, 457–470 (1997).
8. P. B. Jamieson, S. C. Abrahams, and J. L. Bernstein, "Ferroelectric tungsten bronze-type crystal structures. I. barium strontium niobate $Ba_{0.27}Sr_{0.75}Nb_2O_{5.78}$," J. Chem. Phys. **48**, 5048–5057 (1968).
9. J. Dec, W. Kleemann, Th. Woike, and R. Pankrath, "Phase transitions in $Sr_{0.61}Ba_{0.39}Nb_2O_6:Ce^{3+}$: I. Susceptibility of clusters and domains," Eur. Phys. J. B **14**, 627–632 (2000).
10. P. Lehnen, W. Kleemann, Th. Woike, and R. Pankrath, "Phase transitions in $Sr_{0.61}Ba_{0.39}Nb_2O_6:Ce^{3+}$: II. Linear birefringence studies of spontaneous and precursor polarization," Eur. Phys. J. B **14**, 633–637 (2000).
11. V. Westphal, W. Kleemann, and M. D. Glinchuk, "Diffuse phase transition and random-field-induced domain states of the 'relaxor' ferroelectric $PbMg_{1/3}Nb_{2/3}O_3$," Phys. Rev. Lett. **68**, 847–850 (1992).
12. W. Kleemann, "Random-field induced antiferromagnetic, ferroelectric and structural domain states," Int. J. Mod. Phys. B **7**, 2469–2507 (1993).
13. J. Dec, W. Kleemann, V. Bobnar, Z. Kutnjak, A. Levstik, R. Pirc, and R. Pankrath, "Random field Ising type transition of pure and doped SBN from the relaxor into the ferroelectric state," Europhys. Lett. **55**, 781–787 (2001).
14. W. Kleemann, J. Dec, P. Lehnen, R. Blinc, B. Zalar, and R. Pankrath, "Uniaxial relaxor ferroelectrics: the random-field Ising model materialized at last," Europhys. Lett. **57**, 14–19 (2002).
15. P. Yeh, *Introduction to Photorefractive Nonlinear Optics* (Wiley, New York, 1993).
16. P. Yeh, "Theory of unidirectional photorefractive ring oscillators," J. Opt. Soc. Am. B **2**, 1924–1928 (1985).
17. D. Kip, S. Aulkemeyer, K. Buse, F. Mersch, R. Pankrath, and E. Krätzig, "Refractive indices of $Sr_{0.61}Ba_{0.39}Nb_2O_6$," Phys. Status Solidi A **154**, K5–K7 (1996).
18. U. B. Dörfler, R. Piechatzek, Th. Woike, M. K. Imlau, V. Wirth, L. Bohatý, T. Volk, R. Pankrath, and M. Wöhlecke, "A holographic method for the determination of all linear electrooptic coefficients applied to Ce-doped strontium-barium-niobate," Appl. Phys. B **68**, 843–848 (1999).